From erosion to bombardment-induced growth on Ir(111)

Ansgar Petersen,[1,*] Carsten Busse,[1] Celia Polop,[1] Udo Linke,[2] and Thomas Michely[1]
[1]*I. Physikalisches Institut, RWTH Aachen, 52056 Aachen, Germany*
[2]*ISG 3, Forschungszentrum Jülich, 52425 Jülich, Germany*
(Received 19 May 2003; published 12 December 2003)

The morphology of the ion bombarded Ir(111) surface is studied using scanning tunneling microscopy. At a temperature of 880 K and ion fluences of the order of 10^{17} ions/m^2 the experiments show a transition from an erosion regime to a bombardment-induced growth regime with increasing ion energy at energies of a few keV. In dependence of ion fluence, for energies exceeding a few keV a transition from bombardment-induced growth to erosion is observed. The growth effect is caused by the bombardment-induced formation of bulk vacancy clusters, remaining at the bombardment temperature still stable against diffusion and annealing at the surface. Annealing experiments show a gradual decrease of bombardment-induced subsurface damage with increasing temperature. Ion energy, ion fluence, and temperature dependence of the growth phenomenon are explained in terms of an effective damage area below the surface.

DOI: 10.1103/PhysRevB.68.245410 PACS number(s): 68.35.Bs, 61.80.Jh, 68.55.Ln, 81.15.−z

I. INTRODUCTION

Ion bombardment is a powerful means for surface nanostructuring. Depending on the material, ion energy, fluence, and angle of incidence regular patterns of craters, grooves, ripples, or dots may be created.[1–6] By atomic scale studies during the recent years it became evident that the formation and evolution of these nanostructures is intimately linked to the temperature-dependent balance of defect production and defect annealing.

Focusing on ion bombardment of metal surfaces at not too low temperatures and not too high ion energies (<1 keV) the zeroth-order description of the surface morphological evolution is the picture of inverse homoepitaxy. The sputtered atoms leave surface vacancies behind, which are mobile in the surface layer and agglomerate at surface vacancy islands. Due to an asymmetry in the annealing of the surface vacancies at step edges—similar to the Ehrlich-Schwoebel barrier for adatoms[7,8]—continued erosion leads to the formation of craters. These craters coarsen during continued bombardment, develop facets and lateral order. While this picture is to a certain approximation fulfilled for a number of well-investigated experimental situations,[9–11] it has a strong implicit assumption. The damage created by the bombarding ions—bulk vacancies and vacancy clusters, interstitials, surfaces vacancies and surface vacancy clusters, adatoms and adatom clusters—anneals by effective bulk and surface diffusion such that the only damage species left is the surface vacancy due to the sputtered material. Of course, this picture must fail whenever the surface and bulk diffusion of the damage is limited and damage annealing is hampered.

Historically one of the most important failures of the inverse homoepitaxy picture for metal erosion is signified by the discovery of target adatom production due to ion bombardment, the phenomenon that besides surface vacancy islands due to sputtering adatoms islands are also formed on the original surface due to atoms pushed onto the surface layer.[9,12] The visualization of the adatom production by variable temperature scanning tunneling microscopy (STM) allowed quantitative studies on the energy and projectile species dependence of adatom production, to image even the adatom damage patterns of single-ion impacts and measure the temperature dependence of the annealing of the bulk damage to the surface by changes in the adatom coverage.[13–19] These measurements provide a key element of the experimental basis for our current understanding of ion bombardment damage of metal surfaces, which distinguishes two scenarios in dependence of the primary energy.

Up to a few hundred eV, damage production may still be adequately described by a binary collision picture. In the impact influenced volume the primary particle gives rise to the formation of single interstitial atoms, bulk vacancies, surface vacancies, and adatoms. The interstitial atoms readily anneal to the surface at temperatures corresponding to a few percent of the melting temperature T_m. Bulk vacancy diffusion sets in at about $0.2\,T_m$ in face-centered-cubic (fcc) metals and terminates the annealing of the bulk damage to the surface.[20,21] With the onset of the mobility and/or dissociation of the adatom clusters and islands [at about $0.3\,T_m$ on fcc(111) surfaces[1]] the sputtered material in the form of surface vacancy islands is the only damage left. Therefore for bombardment temperatures $\geqslant 0.3\,T_m$ and at low ion energies the inverse homoepitaxy picture is a reasonable approximation for the surface morphological evolution.

In the keV primary ion energy range however, the situation becomes, more complex. The energy density created by the primary particle becomes now sufficient to melt the central part of the impact influenced volume. Due to the lower density of the liquid this thermal spike expands and melt flows onto the initial surface.[22,23] Because of the heat conduction into the surrounding the melt cools until the undercooled liquid rapidly solidifies from the phase boundaries leaving a vacancy rich core of vacancy clusters below the surface and a huge number of adatoms in adatom clusters on the surface. The number of adatoms generally exceeds the number of sputtered atoms by far. Annealing of the ion bombardment damage formed in consequence of a thermal spike requires generally a higher temperature than the above de-

scribed low-energy damage formed in the absence of a spike.[16] Specifically if the vacancy clusters formed are not connected to the surface, i.e., situated well below it, considerably higher temperatures for damage annealing than $0.3\,T_m$ are required.[19] If the vacancy clusters do not diffuse as an entity (with a size dependent, higher activation energy compared to single-bulk vacancies) they can only anneal by dissociation of vacancies from the clusters which takes place only at about $0.45\,T_m$.[20,21]

The present study is motivated by two apparently contradictory results for low fluence ion bombardment of two fcc metals at identical scaled melting temperatures at the onset of the spike regime. Ion bombardment of Pt(111) by 1-keV Xe^+ at 650 K ($0.32\,T_m$) leads to a clear vacancy island erosion morphology.[1,10] Complete damage annealing to the surface is just achieved. Ion erosion of Al(111) by 1-keV Xe^+ at 300 K (the same scaled temperature of $0.32\,T_m$) results in bombardment-induced growth.[18,19] Instead of vacancy islands *only* large adatoms islands are visible on the original surface. Although surface diffusion is highly efficient at this temperature for Al(111) instead of the majority defect (the vacancy) the minority defect species (the adatom) is visible at the surface. Evidently large, stable, and immobile bulk vacancy clusters remain below the surface. It was concluded that the different behavior of the two metals is primarily caused by the different depth of melt formation, which for Al is located much deeper below the surface than for Pt(111) due to the much smaller stopping power of Xe in Al. Thus, while for Al efficient separation of the vacancy clusters from the surfaces takes place, it may be that for Pt(111) the shallow damage leaves the vacancy clusters created in connection to the surface, allowing surface diffusion (with a lower onset temperature than bulk vacancy cluster diffusion or dissociation) to anneal the damage leaving thus only surface vacancy islands representing the net removed material.

One may speculate that both morphologies, the vacancy island erosion morphology and the bombardment-induced growth, may be realized for a single system at a fixed temperature by tuning the primary ion energy and thus the melt and damage depth. For this purpose we present here a systematic study for low fluence bombardment morphologies of Ir(111) at 880 K (corresponding to the $0.32\,T_m$ used also for Pt and Al measurements) in dependence of ion energy and ion fluence, complemented by damage annealing measurements.[36]

II. EXPERIMENT

All experiments were carried out in an ultrahigh vacuum variable temperature STM system with a base pressure below 5×10^{-11} mbar, described in detail elsewhere.[24] A clean Ir(111) surface was prepared by prolonged ion bombardment with a mass selected 1.5-keV Xe^+ beam at 850 K, terminated by annealing to 1570 K. The resulting average terrace width is about 500 Å.

For the bombardment experiments Xe^+, Xe^{++}, and Xe^{+++} ions were accelerated by up to 5 kV. To establish bombardment energies up to 5-keV Xe^+, for 10-keV Xe^{++} and for 15-keV Xe^{+++} ions were used. The ion fluence F_{ion} is given in units of monolayers (ML). For Ir(111) 1 ML $=1.58\times10^{19}$ atoms/m^2. For the experiments the fluence was varied between 2.0×10^{-5} ML and 0.048 ML. The ion flux was varied between 1.0×10^{-4} ML/s and 6.4×10^{-4} ML/s to keep the irradiation time whenever possible at 60 s. All experiments were performed at normal ion incidence. The experimental procedure was as follows. The ion beam was adjusted and the ion flux then measured in a Faraday cup. Subsequently the sample was heated to the bombardment temperature and moved into the ion beam. After the desired ion fluence was reached the sample was removed from the beam and heating was switched off. After controlling the ion flux again the ion beam was also switched off. Eventually, after the sample had cooled to room temperature STM imaging started.

The STM images were recorded as gray scale topographs for quantitative image analysis and as differentiated topographs allowing a better visualization of the stepped surface. Differentiated topographs, which appear as if illuminated from the left, are shown here.

III. RESULTS

Figure 1 shows the surface morphologies after Xe^+ ion bombardment with different ion energies E_{ion} and ion fluences F_{ion} at 880 K. Besides few preexisting steps present already prior to bombardment (steps crossing the entire topograph) the morphologies are dominated by adatom and vacancy islands. Diffusion of both, adatoms[25,26] and surface vacancies is activated at 880 K and allows agglomeration of the defects created by many impacts to extended islands. It should be noted that not only adatoms or surface vacancies are mobile at 880 K but also clusters of these species.[25,27] The compact, nearly hexagonal islands shapes prove the presence of step edge diffusion,[28] which allows the islands to obtain a shape close to their equilibrium shape.[29] At the temperature under concern transport between different atomic layers (e.g., the descent of adatoms into vacancy island edges[30]) is also activated, such that diffusion has already reduced the extent of adatoms and surface vacancies initially produced by the ion impacts. As interstitial diffusion and bulk vacancy diffusion have onset temperatures of 50 K (Ref. 31) and 300 K (Ref. 32) the only damaged species that might be present but invisible for the STM is the bulk vacancy cluster below the surface. While nothing is known about the diffusion of bulk vacancy clusters, their dissociation is not yet terminated after annealing to 1170 K.[33]

A. Dependence of surface morphology on ion energy

First of all a look shall be taken upon how the surface morphology changes with increasing ion energy (from left to right in one row) for different fluences. The evolution of the surface morphology with increasing ion energy is qualitatively similar for the different fluences shown. As the series with $F_{ion}=0.012$ ML exhibits the largest energy range, it is described in more detail.

After bombardment with 0.5-keV Xe^+ ions only small vacancy islands of monatomic depth are observable in Fig.

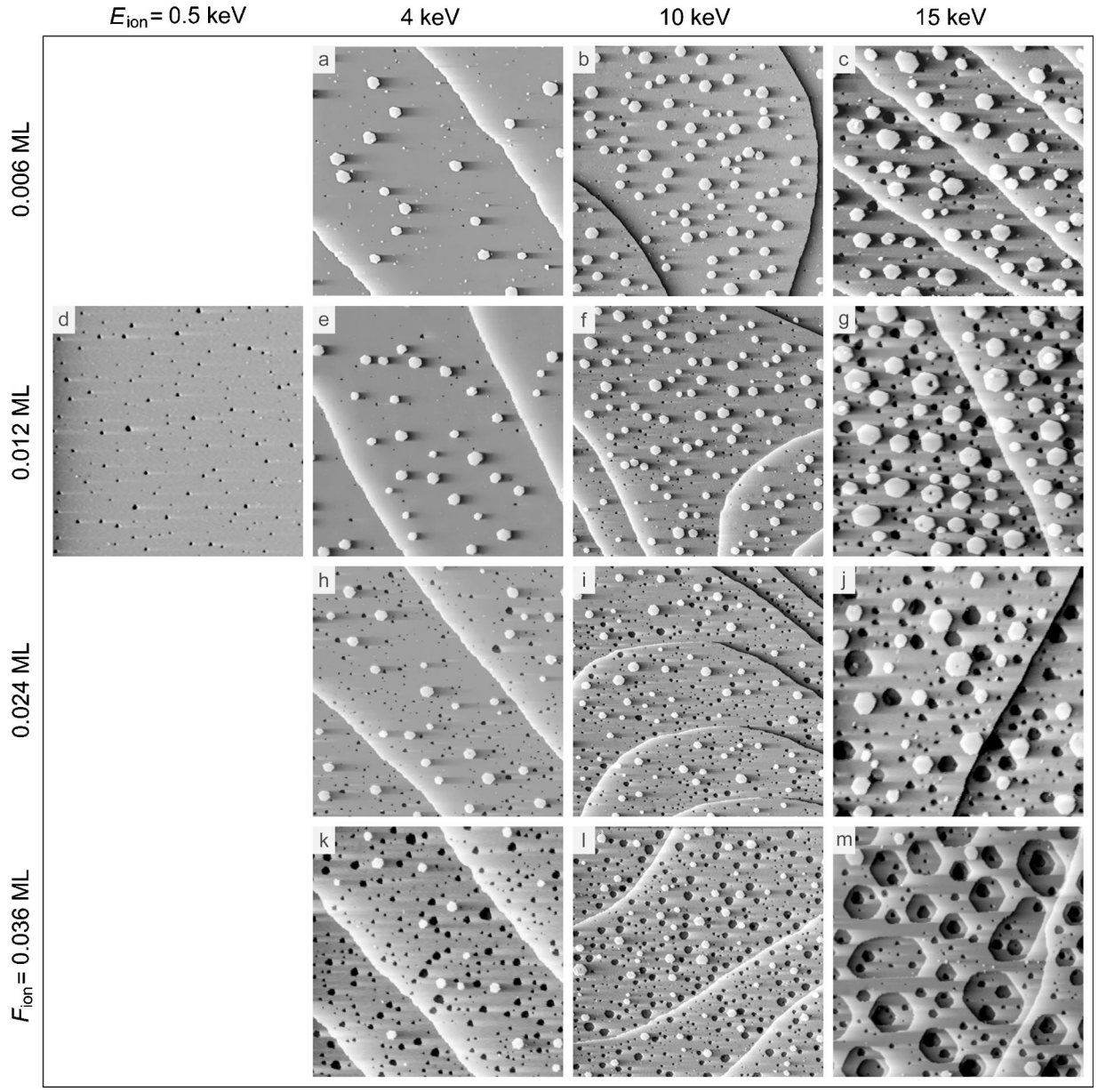

FIG. 1. STM topographs of the Ir(111) surface after ion bombardment at 880 K with Xe ions. From the leftmost to the rightmost column the energy increases from 0.5 keV to 15 keV. The ion fluence F_{ion} increases from the top to the bottom row from 0.006 ML to 0.036 ML. The original surface is in all pictures identifiable as the cohesive layer. A step present prior to bombardment crosses an entire topograph. STM images were recorded after the sample had cooled to nearly room temperature. All topographs are of the size 1100×1100 Å^2.

1(d). On the average, each vacancy island contains about 10–15 surface vacancies. Increase of the ion energy to 1 keV causes adatom islands to show up sporadically, while the surface vacancy islands remain dominant (picture not shown). At $E_{\mathrm{ion}}=4$ keV, [Fig. 1(e)] an adatom island morphology is observed with only small sparse vacancy islands in between. The area of the adatom islands outweighs the vacancy island area by far. In order to ensure the mass balance, there have to be a lot of large, stable bulk vacancy clusters hidden below the surface. Comparison of Figs. 1(d) and 1(e) displays the transition from erosion to bombardment-induced growth by increasing ion energy. We establish here, to our knowledge, for the first time, that both regimes may be realized for the same combination of primary ion and target material by simply tuning the ion energy. Increasing E_{ion} to 10 keV [Fig. 1(f)] causes an increase in the number of adatom islands. Their total area increases significantly, but at the same time vacancy islands also become visible in larger number. At the highest investigated ion energy of $E_{\mathrm{ion}}=15$ keV [Fig. 1(g)] the adatom island covered area increases again, but now vacancy islands also become a prominent feature of the morphology. The surface is considerably roughened. Comparing the different rows of Fig. 1 it is apparent that with increasing ion fluence the energy evolution becomes a more erosive character and for the largest applied fluence $F_{\mathrm{ion}}=0.036$ ML the morphology is dominated by vacancy islands at all energies applied [Figs. 1(k)–1(m)].

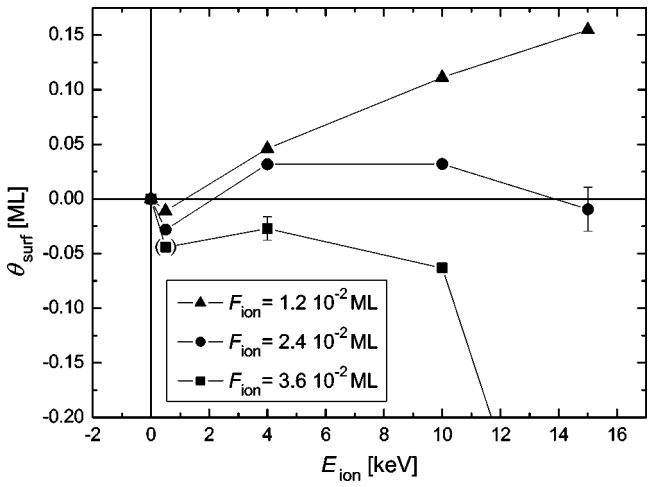

FIG. 2. Change of surface coverage θ_{surf} in dependence of ion energy E_{ion} for different ion fluences $F_{ion}=0.012$ ML (▲), $F_{ion}=0.024$ ML (●) and $F_{ion}=0.036$ ML (■). All experiments were performed at 880 K. One can notice the change from an erosion regime at $E_{ion}<E_{crit}$ ($\theta_{surf}<0$) to a growth regime [(▲), (●)] for $E_{ion}>E_{crit}$ ($\theta_{surf}>0$) with 1 keV$<E_{crit}<$2.5 keV. Only for (■) growth is averted due to high F_{ion}. The missing point of (■) is $\theta_{surf}=-0{,}47$ ML at $E_{ion}=15$ keV. The bracketed point is extrapolated from the two measurements with lower F_{ion} at equal E_{ion}. If error bars are not visible, they are smaller than the according symbol.

In analyzing the topography, the change in surface coverage θ_{surf} is calculated. It is defined as $\theta_{surf}=\Sigma_i i\theta_i$, whereas i stands for the number of the particular atomic layers above ($i>0$) or below ($i<0$) the original surface ($i=0$) and θ_i is the uncovered open part of layer i in monolayer. An accumulation of material on top of the surface is characterized by $\theta_i>0$ (growth), while $\theta_i<0$ represents erosion of material from the surface.

The quantitative dependence of θ_{surf} on the ion energy is plotted in Fig. 2 for three different ion fluences. For all fluences below a critical ion energy E_{crit} around 1-keV erosion prevails, while for energies $E_{ion}>E_{crit}$ growth may take place. The more pronounced, the lower the growth the F_{ion}. The amount θ_{surf} increases nearly linear for $F_{ion}=0.012$ ML, goes through a maximum at about 6 keV for $F_{ion}=0.024$ ML and is absent for $F_{ion}=0.036$ ML, though the increase of θ_{surf} from 0.5 keV to 4 keV is still a reminiscent of bombardment-induced growth. The nearly linear increase of θ_{surf} for the lowest fluence may be rationalized by the linear increase of the melt volume inside the thermal spike.[21,34] An explanation for a degression of bombardment-induced growth with ion energy at the intermediate fluence of $F_{ion}=0.024$ ML and its absence for $F_{ion}=0.036$ ML is postponed to the discussion.

B. Dependence of surface morphology on ion fluence

If one again takes a look at Fig. 1, but now follows the topographs of one column (fixed E_{ion}) with increasing F_{ion} [for example, from Fig. 1(a) to Fig. 1(k)], after an initial slight raise of the adatom island number density the erosion

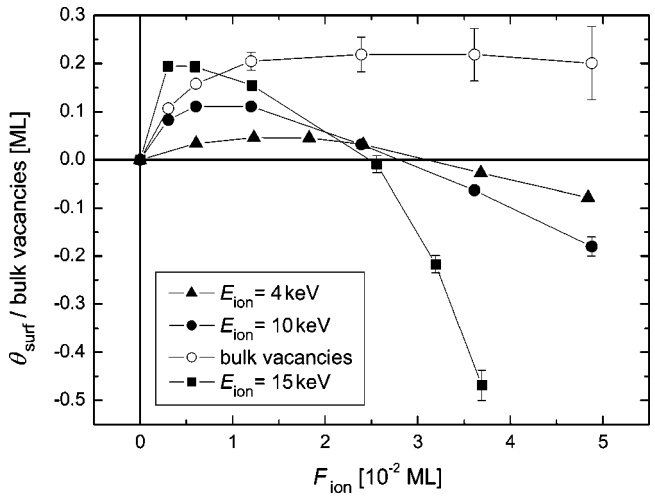

FIG. 3. Change of surface coverage θ_{surf} in dependence of ion fluence F_{ion} for three different ion energies: $E_{ion}=4$ keV (▲), $E_{ion}=10$ keV (●), and $E_{ion}=15$ keV (■). All experiments have been performed at $T_{sample}=880$ K. Additionally the amount of bulk vacancies produced is shown for the $E_{ion}=10$-keV experiment (○).

becomes more and more pronounced with an increasing number and total area of vacancy islands and a decreasing number and area of adatom islands. Most pronounced is the erosion in Fig. 1(m), where adatom islands can be observed only sporadically, while large, up to 3 ML, deep craters have evolved.

A quantitative analysis of θ_{surf} with fluence F_{ion} for three different ion energies is shown in Fig. 3. A maximum value $\theta_{surf,max}$ for θ_{surf} can be estimated for each ion energy and is given in Table I. The fluence F^*_{ion} at which the maximum growth is reached decreases with increasing energy. Moreover the magnitude of $\theta_{surf,max}$ gains in height with increasing ion energy. Increasing the fluence beyond F^*_{ion} initiates a decrease of θ_{surf} leading to a regime of linear decrease for the two lower-energy curves of 4 keV and 10 keV. The linear decrease for large F_{ion} can be explained by the saturation of the subsurface impact influenced layer with bulk vacancies and bulk vacancy clusters. As the average number of bulk vacancies stays constant from this point on, sputtering causes a linear erosion rate. Thus from the slope of the θ_{surf} versus F_{ion} curves at the high fluence end the sputtering yield Y_{sp} (mean number of sputtered atoms per impinging ion) can be calculated for 4 keV and 10 keV (compare Table I). For $E_{ion}=15$ keV, only a lower boundary of Y_{sp} can be given,

TABLE I. Maximum values of change in surface coverage $\theta_{surf,max}$ and corresponding ion fluences F^*_{ion}. Calculated sputtering yields Y_{sp}.

E_{ion} (keV)	$\theta_{surf,max}$ (10^{-2} ML)	F^*_{ion} (10^{-2} ML)	Y_{sp}
0.5			1.1 ± 0.2
4	4.6 ± 0.1	1.5	4.5 ± 0.1
10	11.1 ± 0.1	0.9	9.2 ± 1.5
15	19.5 ± 0.1	0.45	$>50\pm10$

TABLE II. Maximum number of bulk vacancies $\theta_{bv,max}$ and adatom yields Y_{ad} for different E_{ion}.

E_{ion} (keV)	$\theta_{bv,max}$ (ML)	Y_{ad}^{eff}
4	0.14 ± 0.01	17
10	0.22 ± 0.04	46
15	>1.4	>137

because saturation with bulk vacancies is not reached completely in the investigated fluence range (the θ_{surf} versus F_{ion} does not reach a linear slope at the high fluence end).

With the knowledge of Y_{sp} the amount of bulk vacancies θ_{bv} now can be calculated using the following equation, which simply expresses the conversation of mass:

$$Y_{sp} + Y_{ad} = Y_{sv} + Y_{bv}, \tag{1}$$

where Y_{ad} denotes the adatom yield (mean number of adatoms produced per impinging ion), Y_{sv} the yield of surface vacancies, and Y_{bv} the yield of bulk vacancies. Multiplying Eq. (1) with F_{ion} and combining $(Y_{ad} - Y_{sv})F_{ion} = \theta_{surf}$ leads to

$$\theta_{bv} = \theta_{surf} + Y_{sp}F_{ion}. \tag{2}$$

In Fig. 3 the values of θ_{bv} are displayed, calculated with Eq. (2) for 10-keV ion bombardment. The increasing amount of bulk vacancies saturates at $F_{ion} = 0.012$ ML. The maximum values of $\theta_{bv,max}$ for $E_{ion} = 4$ keV and 10 keV are displayed in Table II. Again, for $E_{ion} = 15$ keV only a lower bound can be given as saturation is not yet achieved.

Another relevant parameter can be calculated from the graphs course of Fig. 3. Near to the origin, the effective adatom yield can be estimated as $Y_{ad}^{eff} = \theta_{surf}/F_{ion} + Y_{sp}$. Analyzing θ_{surf}/F_{ion} for the lowest fluence data point ensures that impact overlap diminishes the apparent amount of adatoms only to a small extent. The results for Y_{ad}^{eff} calculated with Y_{sp} from Table I are shown in Table II.

However, even in the complete absence of impact overlap the effective adatom yield Y_{ad}^{eff} (880 K) measured after bombardment at 880 K is by far smaller than the true adatom yield Y_{ad}, which is the number of adatoms pushed onto the surface during the energetic phase of a few picoseconds after the impact. At nonzero temperatures the combined action of surface and bulk diffusion will lead to a partial annealing of the produced adatoms. For bombardment at 880 K the majority of adatoms is already annealed by bulk vacancies and bulk vacancy clusters reaching the surface and subsequent filling with adatoms. Single-ion impact experiments with 10-keV ions performed at 300 K with the low fluence of $F_{ion} = 2 \times 10^{-5}$ ML illustrate these facts. Figure 4 shows large clusters of adatoms surrounding each impact point, whereas the impacts are separated far enough not to influence each other. With the adatom islands being of monoatomic height, Y_{ad}^{eff} (300 K) $= 370 \pm 40$ is determined from the island area per impact, which is by about a factor of 8 larger than the corresponding 10-keV value Y_{ad}^{eff} (880 K) obtained after bombardment at 880 K.

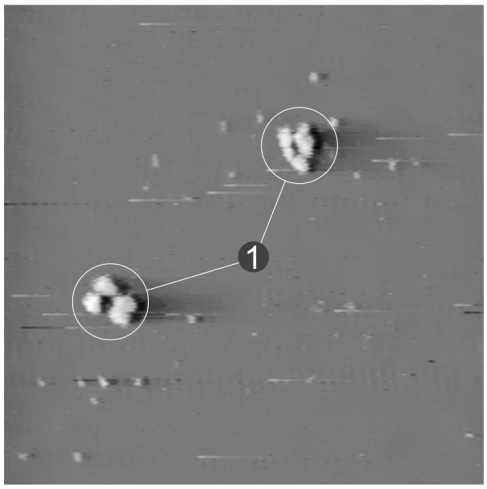

FIG. 4. Single-ion impacts on the Ir(111) surface after bombardment with 10-keV Xe ions at a ion fluence of $F_{ion} = 2 \times 10^{-5}$ ML, $T_{sample} = 300$ K: (1) adatom island surrounding two impact points. STM image is recorded at room temperature, picture of size 670×670 Å^2.

C. Annealing experiments

Additional information about the temperature-dependent behavior of vacancies and vacancy clusters created below the surface by ion bombardment is obtained by annealing experiments. Bombardment of the surface at 350 K was followed by a sequence of successively higher annealing intervals of 60 s duration with intermittent room temperature STM imaging. An extract of the topographs gained in these experiments is shown in Fig. 5. Figures 5(d)–5(f) show the annealing behavior after 0.5-keV bombardment, while the complete analysis of this experiment is shown as down triangles in Fig. 6. In Fig. 5(d) a large number of small vacancy islands and a few adatom islands are visible. Even at the low temperatures used here the low ion energy does not allow to reach the growth domain. The existence of a few adatom islands after 0.5-keV bombardment at 350 K and their absence after bombardment at 880 K in Fig. 1(d) is due to the hampered transport of adatom and adatom clusters over descending step edges resulting in their annihilation. Annealing of the sample leads to complete adatom island annihilation [Fig. 5(e)] and a gradual decrease of the vacancy island density together with their growth. The observed vacancy island coarsening is due to Brownian motion causing island coalescence accidentally.[35] The quantitative analysis in Fig. 6 makes it obvious that the vacancy covered island area is continuously increasing with increasing annealing temperature. No distinct annealing steps are visible. As single-bulk vacancies are mobile already at 300 K,[32] all single-bulk vacancies created have reached the surface by random walk already during the initial bombardment interval. Since bulk vacancy clusters only dissociate significantly at temperatures above 1170 K (Ref. 33) the most probable explanation for the gradual increase of θ_{surf} is the gradual onset of bulk vacancy cluster mobility. With increasing temperature larger and larger bulk vacancy clusters become mobile, which arrive during their random walk at the surface, where they

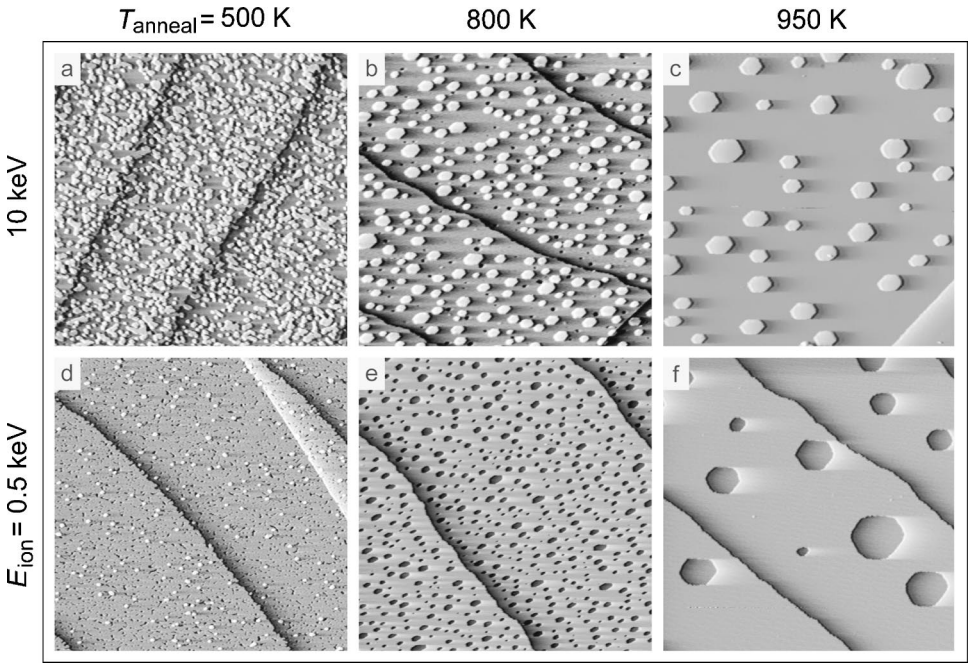

FIG. 5. STM topographs of the Ir(111) surface after bombardment at 350 K with Xe ions of 10 keV energy (a–c) at a ion fluence of $F_{ion}=0.006$ ML and with Xe ions of 0.5 keV energy (d—f) at a ion fluence of $F_{ion}=0.18$ ML, annealed to the denoted temperatures of 500 K, 800 K, and 950 K. STM images are recorded at room temperature. All topographs are of the size 1100×1100 Å^2.

anneal to form surface vacancy islands. After 0.5-keV bombardment, the saturation in θ_{surf} around 1000 K suggests nearly complete bulk damage annealing. Thus from θ_{surf} measured after annealing to 1100 K the sputtering yield for 0.5-keV Xe^+ bombardment is estimated to $Y_{sp}\approx1.3$.

A similar decrease of θ_{surf} with the annealing temperatures is found after 10-keV ion bombardment in Figs. 5(a)–5(c) and the quantitative analysis in Fig. 6 (up triangles). The main difference compared to the 0.5-keV bombardment is that the entire annealing sequence is situated in the growth domain with $\theta_{surf}>0$ ML for all temperatures. Again no steps are visible in the decrease of θ_{surf} with increasing T_{anneal}. The overall higher θ_{surf} tells that an overall larger amount of bulk vacancy clusters was created below the surface. The much larger slope at the high temperature end of the 10-keV annealing curve compared to the 0.5-keV one indicates that annealing for 10 keV is far from being terminated at 1100 K. Extension of the annealing measurements to temperatures above 1100 K is impossible, because thermal generation of adatoms from step edges becomes so efficient that all island structures dissociate and no more damage is visible on the surface. One may estimate, however, that based on $Y_{sp}=9.2$ for 10-keV ion bombardment from Table I for complete annealing $\theta_{surf}=-0.05$ ML is expected. As an explanation for the fact that for 10-keV bombardment even at 1100 K vacancy clusters still remain below the surface we note that due to the larger spike volume the distribution of bulk vacancy clusters can be assumed to be shifted to larger sizes. This implies a shift of the distribution of cluster diffusion temperatures to larger values compared to the 0.5-keV case and thus a need for higher temperatures to achieve complete annealing.

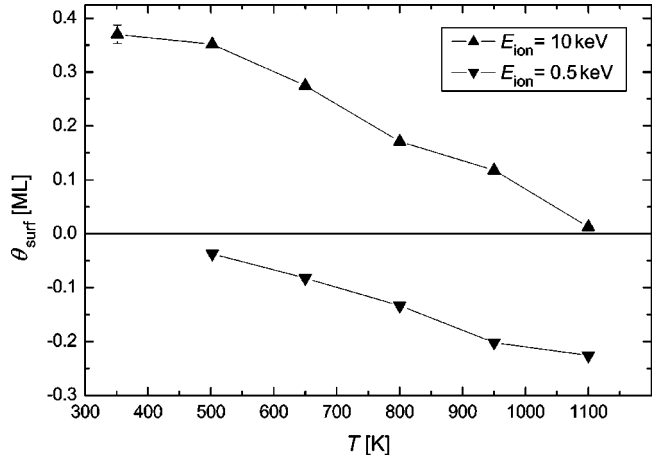

FIG. 6. Change of surface coverage θ_{surf} in dependence of annealing temperature after ion bombardment. $E_{ion}=10$ keV, $F_{ion}=0.006$ ML (▲) and $E_{ion}=0.5$ keV, $F_{ion}=0.18$ ML (▼).

D. Temperature dependence of bombardment-induced growth

The annealing experiments discussed in the preceding section suggest that the bombardment-induced growth depends sensitively on temperature. Figure 7 compares the dependence of θ_{surf} with E_{ion} for a fixed fluence of $F_{ion}=0.036$ ML at two different temperatures, 800 K and 880 K. The difference in surface evolution caused by the different bombardment temperatures is remarkable. While at 800 K still pronounced growth with a maximum $\theta_{surf,max}=0.15$ ML takes place, bombardment-induced growth is absent at 880 K, though the increase of θ_{surf} from 0.5 keV to 4 keV is still a reminiscent of growth. Beyond the initial erosion regime for low temperatures, the difference in θ_{surf} for the two temperatures increases with the ion energy and reaches at 10-keV values of about 0.2 ML. An explanation consistent with the annealing experiments is provided by the temperature dependence of the *stable* cluster volume created per impact. The lower is the temperature the larger is this volume, as at lower temperatures smaller bulk vacancy clusters remain immobile and thus stable below the surface.

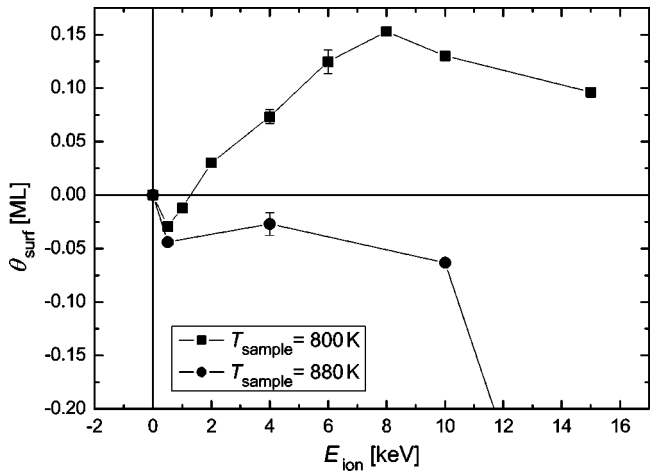

FIG. 7. Evolution of θ_{surf} with E_{ion} for a fluence of $F_{ion}=0.036$ ML at 800 K (■) and 880 K (●).

IV. DISCUSSION

The results obtained so far for the change of θ_{surf} by bombardment at 880 K in dependence of E_{ion} and F_{ion} are summarized in the topographic representation of Fig. 8. The thin dashed line in Fig. 8 separates the domains of bombardment-induced growth and erosion, while the thin full line indicates the position of the ridge of the growth mountain.

A specific ion energy is needed to create bulk vacancy clusters large enough to be thermally stable at 880 K. Thus below a certain threshold energy for all ion fluences erosion takes place. The threshold energy is visible as the vertical part of the domain separation line in Fig. 8. It is associated with the achievement of a sufficient energy density for spike formation and of a sufficient depth of the spike such that the vacancy clusters are created below the surface, disconnected from it. The fluence dependence of Fig. 8 may be rationalized by the concept of a damage area A_{damage} associated with each impact. The damage area is the projection of the impact influenced layer below the surface onto the surface within which vacancies and vacancy clusters are created. Assuming for simplicity a uniform distribution of impacts over the surface, the layer below the surface is saturated with vacancies and vacancy clusters after an ion dose $F_{ion}^{sat}=1/A_{damage}$, if A_{damage} is measured in lattice sites. For a fixed ion energy, at this ion fluence the maximum growth effect is reached (the ridge of the growth mountain), i.e., $F_{ion}^{sat}=F_{ion}^{*}$. As an example, in this picture saturation with bulk vacancies after about $F_{ion}^{*}=0.9\times10^{-2}$ ML for 10-keV bombardment (compare Fig. 3 and Table I) implies a damage area of about 110 lattice sites with a diameter of about 30 Å. Increasing the fluence beyond bulk damage saturation leads over to erosion, as no net material transport from the bulk to the surface takes place and at the same time material is sputtered away from the surface. In our simplified picture we may assume that after saturation of the bulk with vacancy clusters at F_{ion}^{*} the quantity θ_{surf} decreases linearly with Y_{sp} such that after a fluence

$$F_{ion}^{0}=\frac{1}{A_{damage}}+\frac{\theta_{surf,max}}{Y_{sp}} \tag{3}$$

the domain boundary between growth and erosion defined by $\theta_{surf}=0$ is reached.

As the primary ion energy increases, A_{damage} increases. Thus with increasing ion energy, bulk vacancy cluster saturation takes place for smaller and smaller fluences. Therefore the ridge of the growth mountain in Fig. 8 is reached for smaller and smaller fluences. The ridge of the growth mountain and the domain separation line are nearly parallel. Apparently $\theta_{surf,max}$ and Y_{sp} increase in a similar way with ion energy [compare Eq. (3)].

For sufficiently small fluences with $F_{ion}\ll 1/A_{damage}$ the increase of θ_{surf} with E_{ion} represents essentially the increase in the volume of stable bulk vacancy clusters created per impact. As long as the nuclear stopping power increases with energy, the viscous outflow of material will increase[23,22] (compare the lowest part of Fig. 8). When at energies $E_{ion}>15$ keV the maximum of the stopping power for Xe ions in Ir is reached, θ_{surf} will reach a maximum as well. Contrary, for sufficiently large fluences fulfilling the condition $F_{ion}\gg 1/A_{damage}$ already for energies at the onset of spike forma-

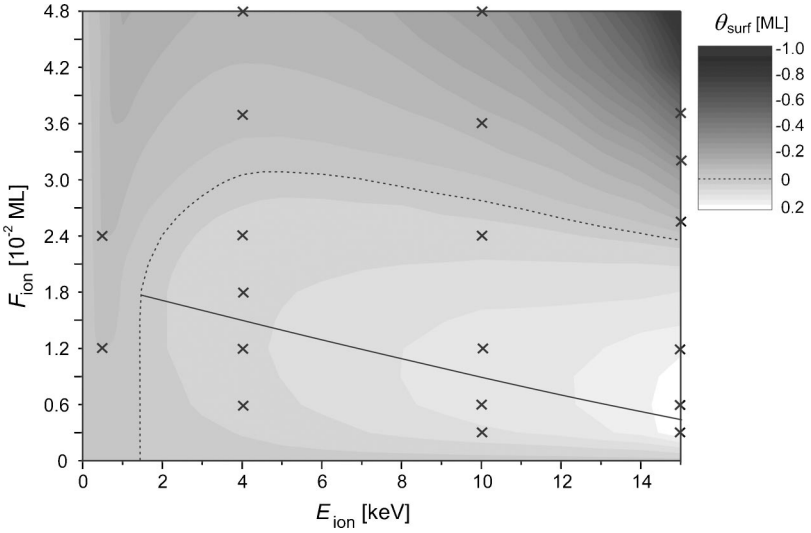

FIG. 8. Dependence of bombardment-induced surface coverage change θ_{surf} on ion energy E_{ion} and ion fluence F_{ion} in a topographic representation. The dashed line marks the transition between erosion ($\theta_{surf}<0$) and growth ($\theta_{surf}>0$). The full line marks the ridge of the growth mountain. The lighter the gray shading within the growth area, the stronger is the growth effect. Accordingly the darkest gray tones (upper right corner) show the area of strongest erosion. Crosses mark the experimentally measured values of θ_{surf}. The topography is formed to best fit these points by interpolating the graphs of Figs. 2 and 3.

tion, the surface remains for all energies in the erosion regime as seen in the upper part of Fig. 8.

Up to now the discussion of the results is restricted to a temperature of 880 K. It is instructive on the shape of Fig. 8 at lower temperatures to guess based on the annealing measurements and the dependence of θ_{surf} on ion energy at two different temperatures (Fig. 7). An obvious conclusion from the annealing measurements shown in Figs. 5 and 6 as well as from Fig. 7 is that only a small fraction of the vacancy volume created by the energetic impacts remains below the surface at elevated temperatures. This conclusion is sustained by comparing the apparent adatom yields at 300 K and 880-K for 10 keV ions, which are 370 and 46, respectively. Therefore the ridge of the growth mountain indicated in Fig. 8 by a thin full line will become considerably higher at lower temperatures (compare also Fig. 7). The growth domain will shift its boundary somewhat towards the left, but there will be a limiting energy associated with the onset of spike formation, somewhere between 0.5 keV and 1 keV beyond which no growth takes place. (Note that growth is still absent for 0.5-keV bombardment at 350 K as shown in Fig. 5.) At first glance, surprisingly, the growth domain also shifts its boundary towards larger ion fluences F_{ion} at lower bombardment temperatures as apparent from Fig. 7. This effect may simply be understood with Eq. (3): while $\theta_{\mathrm{surf,max}}$ increases with decreasing temperature, Y_{sp} is temperature independent. Thus, F^0_{ion} shifts to larger values for all energies and thus the domain separation line upwards in Fig. 8.

V. CONCLUSION

Under proper conditions (ion energy, ion fluence, temperature) bombardment-induced growth must be assumed to take place on every metal surface, also on those for which up to now only erosion morphologies were observed. The systematic study of the growth phenomenon in dependence on ion energy, ion fluence, and temperature presented here allows to predict the proper conditions for the observation of bombardment-induced growth. It is most easy observable at the low fluence, low temperature, and high ion energy limit. The strength of the growth phenomenon at a given temperature depends sensitively on the efficiency of bulk vacancy cluster diffusion. Efficient surface diffusion in the absence of bulk vacancy cluster diffusion leads to a pure growth morphology consisting only of adatom islands, while inefficient surface diffusion leads to a morphology representing adatom islands as well as vacancy islands. The observed dependencies of the growth phenomenon may be rationalized by a damage area A_{damage} which increases with ion energy.

ACKNOWLEDGMENT

This work was supported by the Deutsche Forschungsgemeinschaft via the project ''Atomare Prozesse beim homoepitaktischen Schichtwachstum unter extremen Nichtgleichgewichtsbedingungen.''

*Corresponding author. Present address: Institute for Biomedical Technologies, RWTH Aachen, 52074 Aachen, Germany. Fax: +49-241-8082442. Email address: petersen@hia.rwth-aachen.de

[1] T. Michely, M. Kalff, G. Comsa, M. Strobel, and K.-H. Heinig, Phys. Rev. Lett. **86**, 2589 (2001).
[2] M.V. Ramana Murty, T. Curcic, A. Judy, B.H. Cooper, A.R. Woll, J.D. Brock, S. Kycia, and R.L. Headrick, Phys. Rev. Lett. **80**, 4713 (1998).
[3] S. van Dijken, D. de Bruin, and B. Poelsema, Phys. Rev. Lett. **86**, 4608 (2001).
[4] S. Rusponi, G. Costantini, C. Boragno, and U. Valbusa, Phys. Rev. Lett. **81**, 4184 (1998).
[5] U. Valbusa, C. Boragno, and F. Buatier de Mongeot, J. Phys.: Condens. Matter **14**, 8153 (2002).
[6] S. Facsko, T. Dekorsy, C. Koerdt, C. Trappe, H. Kurz, A. Vogt, and H.L. Hartnagel, Science **285**, 1551 (1999).
[7] G. Ehrlich and F. Hudda, J. Chem. Phys. **44**, 1039 (1966).
[8] R.L. Schwoebel and E.J. Shipsey, J. Appl. Phys. **37**, 3682 (1966).
[9] T. Michely and G. Comsa, Phys. Rev. B **44**, 8411 (1991).
[10] M. Kalff, G. Comsa, and T. Michely, Surf. Sci. **486**, 103 (2001).
[11] G. Costantini, F. Buatier de Mongeot, C. Boragno, and U. Valbusa, Phys. Rev. Lett. **86**, 838 (2001).
[12] R.P. Webb and D.E. Harrison, Jr., Radiat. Eff. Lett. Sect. **86**, 15 (1983).
[13] C. Teichert, M. Hohage, T. Michely, and G. Comsa, Phys. Rev. Lett. **72**, 1682 (1994).
[14] H. Gades and H.M. Urbassek, Phys. Rev. B **50**, 11 167 (1994).
[15] T. Michely and C. Teichert, Phys. Rev. B **50**, 11 156 (1994).
[16] M. Morgenstern and T. Michely, Philos. Mag. A **79**, 775 (1999).
[17] M. Ghaly, K. Nordlund, and R.S. Averback, Philos. Mag. A **79**, 795 (1999).
[18] C. Busse, H. Hansen, U. Linke, and T. Michely, Phys. Rev. Lett. **85**, 326 (2000).
[19] C. Busse, C. Engin, H. Hansen, U. Linke, T. Michely, and H. Urbassek, Surf. Sci. **488**, 346 (2001).
[20] P. Ehrhart, in *Landolt-Börnstein, Neue Serie, Gruppe III*, edited by H. Ullmaier (Springer, Berlin, 1991), Vol. 25, pp. 88–379.
[21] W. Schilling and H. Ullmaier, in *Materials Science and Technology*, edited by W. Cahn, R. P. Haasen, and K. Kramer (Verlag Chemie, Weinheim, 1993), Vol. 10, pp. 180–241.
[22] M. Ghaly and R.S. Averback, Phys. Rev. Lett. **72**, 364 (1994).
[23] R.S. Averback and M. Ghaly, J. Appl. Phys. **76**, 3908 (1994).
[24] T. Michely, *Jül-Bericht 2569* (Forschungszentrum Jülich, Jülich, 1991).
[25] S.C. Wang, U. Kürpick, and G. Ehrlich, Phys. Rev. Lett. **81**, 4923 (1998).
[26] C. Busse, W. Langenkamp, C. Polop, A. Petersen, H. Hansen, U. Linke, P. J. Feibelman, and T. Michely, Surf. Sci. Lett. **539**, L560 (2003).
[27] S.C. Wang and G. Ehrlich, Phys. Rev. Lett. **79**, 4234 (1998).
[28] T.-Y. Fu and T.T. Tsong, Phys. Rev. B **61**, 4511 (2000).
[29] M.J. Rost, T. Michely, and G. Comsa, Phys. Rev. B **57**, 1992 (1998).
[30] S.C. Wang and G. Ehrlich, Phys. Rev. Lett. **67**, 2509 (1991).
[31] P. Petroff and J. Washburn, Phys. Status Solidi **32**, 427 (1969).
[32] A. Hoffmann, A. Willmeroth, and R. Vianden, Z. Phys. B: Condens. Matter **62**, 335 (1986).
[33] J.A. Hudson and B. Ralph, Philos. Mag. A **25**, 265 (1972).

[34] K. Nordlund, M. Ghaly, R.S. Averback, M. Caturla, T.D. de la Rubia, and J. Tarus, Phys. Rev. B **57**, 7556 (1998).

[35] K. Morgenstern, G. Rosenfeld, B. Poelsema, and G. Comsa, Phys. Rev. Lett. **74**, 2058 (1995).

[36] Instead of scaling the behavior of the three mentioned materials Pt, Al, and Ir to their melting temperatures one could also scale with the cohesive energy E_{coh}. The bombardment temperature of 880 K used for Ir corresponds to $1.10\times10^{-2}\ E_{\mathrm{coh}}/kT$, where k is the Boltzmann's constant. The same fraction of the cohesive energy for Pt and Al corresponds to temperatures of 750 K and 435 K, respectively. While Pt(111) exhibits a similar behavior at this higher temperature than at 660 K corresponding to 0.32 T_{m}, for Al(111) the surface diffusion at 435 K is so efficient that all defect structures dissociate, leading to a step-flow growth. However, still at 400 K adatom islands characteristic for bombardment-induced growth could be discerned.